Applied Catalysis B: Environmental 185 (2016) 11–21

Contents lists available at ScienceDirect

Applied Catalysis B: Environmental

journal homepage: www.elsevier.com/locate/apcatb

ZnO rods/reduced graphene oxide composites prepared *via* a solvothermal reaction for efficient sunlight-driven photocatalysis

Hatem Moussa[a,b], Emilien Girot[a], Kevin Mozet[a], Halima Alem[c], Ghouti Medjahdi[c], Raphaël Schneider[a,*]

[a] CNRS and Université de Lorraine, Laboratoire Réactions et Génie des Procédés (LRGP), CNRS UMR 7274, 1 rue Grandville, 54001 Nancy, France
[b] Laboratoire de Biosurveillance de l'Environnement, Université de Carthage, Faculté des Sciences de Bizerte, 7021, Jarzouna, Bizerte, Tunisia
[c] CNRS and Université de Lorraine, Institut Jean Lamour (IJL), UMR CNRS 7198, BP 70239, 54506 Vandoeuvre-lès-Nancy Cedex, France

ARTICLE INFO

Article history:
Received 28 September 2015
Received in revised form
27 November 2015
Accepted 2 December 2015
Available online 4 December 2015

Keywords:
ZnO rods
Reduced graphene oxide
Composite
Solvothermal synthesis
Photocatalysis
Solar light irradiation

ABSTRACT

Small-sized ZnO rods with an average length of *ca.* 180 nm and a diameter of *ca.* 16 nm were successfully associated to reduced graphene oxide (rGO) *via* a solvothermal reaction conducted in ethanol. A set of characterization including TEM, SEM, XRD, BET, Raman spectroscopy and UV–vis absorption confirm that the ZnO/rGO composite is composed of highly dispersed ZnO rods bound to rGO nanosheets. The photocatalytic activity of the ZnO/rGO composite was investigated under solar light and under visible light irradiation using the Orange II dye in aqueous solution. Results indicate that the ZnO/rGO composite containing 10 wt% rGO used under solar light irradiation exhibit the highest photocatalytic activity and that the kinetic of reduction is of pseudo-fist-order. The photocatalyst is only weakly sensitive to pH changes and to the presence of inorganic salts or to glucose in the reaction medium. In addition, the reusability of the ZnO/rGO composite was studied and the results demonstrate that the photocatalyst can be reused up to fifteen times with nearly negligible loss of activity. The high photocatalytic performances can be attributed to the high specific surface of ZnO rods, to the enhanced visible light absorption of the ZnO/rGO composite and to the strong decrease of charge carrier recombinations originating from the association of ZnO rods with rGO.

1. Introduction

Semiconductor mediated photocatalysis is an efficient method for environmental detoxification, which is able of converting toxic and nonbiodegradable organic compounds into carbon dioxide, water and inorganic salts [1–4]. Zinc oxide ZnO is one of the most promising photocatalyst both for solar energy conversion and for the treatment of dyes and organic pollutants due to its weak toxicity, high abundance, chemical and optical stabilities and photocatalytic efficiency [5–9]. The photocatalytic activity of ZnO originates from the photo-generated electrons and holes which are strong reducing and oxidizing agents, respectively.

The design of ZnO particles with controlled morphology at the nanometer scale is an important parameter governing the photocatalytic activity. Indeed, the optical and electrical properties depend highly on the structure, size, shape, defect concentration,... In recent years, various ZnO nanostructures like hexagonal disks and rings [10], rods [11,12], tubes [13], nanoflowers [14],... have easily been prepared *via* wet chemical synthesis routes. Among these nanostructures, ZnO rods have attracted a lot of attention for photocatalytic applications due to their high stability and large specific surface area [15–26].

However, the use of ZnO in visible light is limited due to its wide bandgap (3.27 eV) which limits its response to the UV light, leaving *ca.* 95–97% energy of the solar spectrum unusable. Moreover, the fast recombination of photo-generated charge carriers in ZnO decreases its photocatalytic performances. Therefore, the development of composite materials containing ZnO particles is of high interest to solve these problems.

Carbon-based nanostructures such as carbon nanotubes [27–29] or carbon nanofibers [30,31] have successfully been associated to ZnO to form hybrid materials with new functionalities, valuable for example in photocatalysis. During photocatalysis experiments, these C-based nanostructures will act both as electron-acceptor and as electron-transport materials, will facilitate the migration of photo-generated electrons and hinder the charge recombination and thus extend the lifetime of electron-hole pairs and improve the photocatalytic efficiency [32,33]. Graphene, and espe-

* Corresponding author. Fax: +33 3 83 32 29 75.
E-mail address: raphael.schneider@univ-lorraine.fr (R. Schneider).

http://dx.doi.org/10.1016/j.apcatb.2015.12.007
0926-3373/

cially reduced graphene oxide (rGO), are also good candidates for photocatalytic applications due to their high electron mobility (>15000 $cm^2 V^{-1} s^{-1}$) and to the flexible sheet nature [34]. In recent years, graphene, graphene oxide or rGO were successfully associated to ZnO nanostructures with spherical or pseudo-spherical, nanosheet, flower-like, hexagonal or nanowire morphologies to develop new photocatalysts, adsorbants, photodetectors, electron transfer systems or materials with enhanced mechanical properties [35–46]. Composite materials associating graphene or rGO to ZnO rods have also been developed [47–52]. However, due to the synthesis methods used (sol–gel process under microwave irradiation, hydrothermal conditions or annealing at high temperature), the rods produced were of huge size (up to 5 μm in length and 200 nm in diameter). Small sized rods with weak aspect ratio and high concentration of oxygen defects exhibit a higher photocatalytic activity than large sized ones [53,54].

In this paper, we developed a new solvothermal method for associating small ZnO rods with a length of 180 nm and a diameter of 16 nm to rGO. The composition, morphology and microstructure on ZnO/rGO composites were characterized. The photocatalytic performances of the ZnO/rGO materials were evaluated in the degradation of the Orange II dye under solar light and visible irradiation and compared to ZnO rods. The effects of different parameters such as the amount of catalyst, the pH of the Orange II solution, and the influence of salts and a reducing sugar (glucose) were analyzed. Results obtained highlight that the association of small-sized ZnO rods with rGO affords photocatalysts with high activity. Finally, the ZnO/rGO catalyst could be reused up to 15 times without any loss of activity.

2. Experimental section

2.1. Materials

Graphite powder (Merck), $KMnO_4$ (>99%, Sigma), $Zn(OAc)_2{\cdot}2H_2O$ (>98%, Sigma), H_2O_2 (30%, VWR Chemicals), potassium permanganate (>99%, Sigma), sodium nitrate (>99%, Sigma), H_2SO_4 (reagent grade), L-ascorbic acid (reagent grade, Sigma), sodium hydroxide (>97%, Sigma), and ethanol were used as received without further purification. All solutions were prepared using Milli-Q water (18.2 MΩ cm, Millipore) as solvent.

2.2. Preparation of exfoliated graphene oxide

Graphite oxide was prepared by oxidation and exfoliation of commercially available graphite by a modified Hummer's method [55]. Briefly, 2 g of graphite and 1 g of sodium nitrate were mixed together in a flask kept at 0 °C using an ice bath. Then, 50 mL of concentrated H_2SO_4 were slowly added to the flask and the mixture was stirred for 30 min. 0.3 g of $KMnO_4$ was then added and the mixture further stirred for 30 min. Next, 7 g of $KMnO_4$ were gradually added and stirred for 1 h (the temperature should not exceed 20 °C). The temperature was raised to 35 °C and the solution was stirred for 2 h. Then, 90 mL of H_2O were slowly added (the temperature increased to 70 °C) and the mixture stirred for 15 min, followed by the addition of mixture of 7 mL H_2O_2 and 55 mL of water to reduce the residual permanganate to soluble manganese ions. The resulting suspension was filtered, washed by centrifugation with 5% HCl (2500 rpm, 10 min, 4 times) followed by water (4000 rpm, 10 min, 5 times) and finally dried at 60 °C for 24 h to obtain a brownish graphite oxide powder.

The graphite oxide powder was dispersed in water (1 mg/mL) to obtain a suspension. Then, the suspension was ultra-sonicated for 1 h by probe sonication (amplitude 25%) to obtain a graphene oxide suspension. Finally, the suspension was centrifuged at 5000 rpm for 15 min to collect graphene oxide (GO) pellets. The GO pellets were dried at 60 °C for 24 h before use.

2.3. Reduction of GO

The reduction of GO into rGO was conducted according to the procedure described by Zhang et al. [56] with slight modifications. Briefly, 15 mg of GO were dispersed in 50 mL water at room temperature. L-Ascorbic acid (200 mg) was next added and the mixture stirred for 24 h under ambient conditions. rGO was recovered by centrifugation (4000 rpm for 15 min), washed with water, and dried overnight at 50 °C.

2.4. Solvothermal synthesis of ZnO rods and of ZnO/rGO composites

ZnO rods were synthesized by a same solvothermal method based on the hydrolysis of $Zn(OAc)_2$. Typically, in a three-necked flask equipped with a condenser and a dropping funnel, $Zn(OAc)_2{\cdot}2\,H_2O$ (511 mg) was dissolved in 35 mL ethanol. To this solution, NaOH (466 mg) in 35 mL ethanol was added dropwise and the mixture stirred for 30 min at room temperature. Then, the solution was transferred into a 140 mL Teflon-sealed autoclave and was heated at 160 °C for 24 h. After cooling to room temperature, the ZnO rods were collected by centrifugation, washed two times with water, two times with ethanol, and dried at 50 °C for 15 h. Typically, this procedure affords 150 mg of ZnO rods.

Various ZnO/rGO composites were synthesized by varying the mass of rGO associated to ZnO rods. For the preparation of the ZnO/rGO composite with 10% weight loading in rGO, 15 mg of rGO were used for the synthesis. For the preparation of the composite, rGO was added to the mixture of $Zn(OAc)_2$ and NaOH after the 30 min of stirring. The mixture was sonicated at room temperature for 10 min before heating at 160 °C for 24 h. The purification and drying procedures are similar to those previously described for ZnO rods.

2.5. Photocatalytic degradation of Orange II

The photocatalytic activity was evaluated by the degradation of an aqueous solution of Orange II (10 mg/L) at room temperature under solar light irradiation. In a typical experiment, the ZnO/rGO composite (60 mg) was dispersed in 50 mL Orange II aqueous solution (10 mg/L) and the suspension was magnetically stirred under ambient conditions for 1 h in the dark to reach an adsorption–desorption equilibrium. Under stirring, the suspension was exposed to simulated solar light irradiation produced by Sylvania LuxLine FHO T5 neon tubes. The irradiation fluence was estimated to be 5 mW/cm^2. At certain time intervals, 2 mL of the suspension were extracted and centrifuged (4000 rpm for 2 min) to remove the photocatalyst. The degradation process was monitored by measuring the absorption of Orange II at 485 nm using a UV–vis absorption spectrometer. The visible light irradiation was carried out using the neon tubes previously described and a polycarbonate film was used as the UV cutoff filter.

2.6. Characterization

Transmission electron microscopy (TEM) images were taken by placing a drop of the particles dispersed in methanol onto a carbon film-supported copper grid. Samples were studied using a Philips CM200 instrument operating at 200 kV. High-Resolution TEM (HR-TEM) imaging were performed with a JEOL ARM 200F-Cold FEG (point resolution 0.19 nm) fitted with a GIF Quatum ER. Electron energy loss spectroscopy (EELS) experiments were recorded in scanning transmission electron microscopy (STEM) mode. The

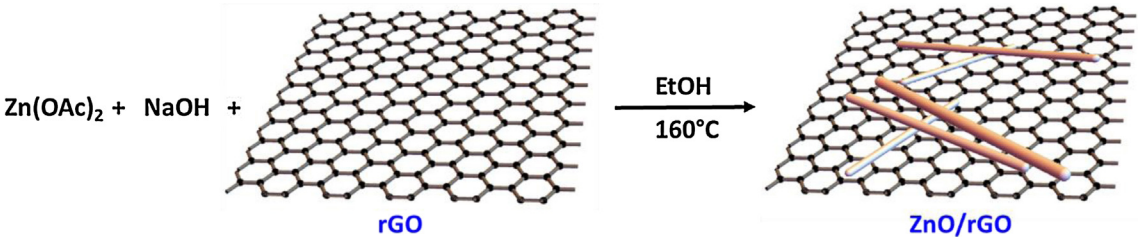

Fig. 1. Schematic illustration of the synthesis of the ZnO/rGO composite.

spectrometer is set to an energy dispersion 0.05 eV/channel. The condenser aperture, spectrometer entrance, camera length were respectively 150 μm, 2.5 mm and 4 cm leading to collection half angle of 20 mrad and an energy resolution of 0.5 eV measured at full width at half maximum (FWHM) of zero loss peak. The energy-filtered images (EF-TEM) were also recorded in STEM mode. Scanning electron microscopy (SEM) pictures were prepared using JEOL Scanning Electron Microscope JSM-6490 LV. The X-ray pow-

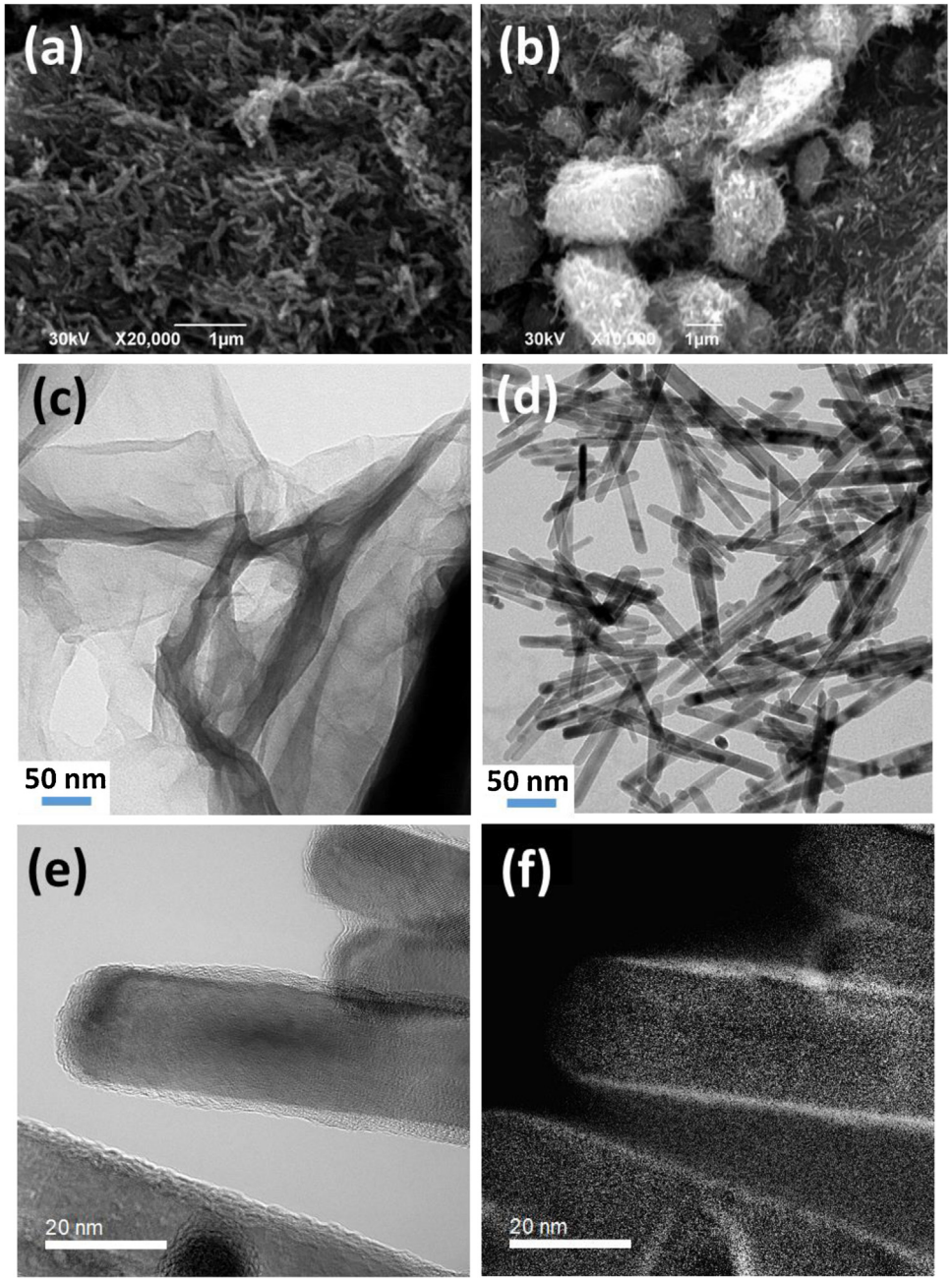

Fig. 2. SEM images of (a) ZnO rods and (b) the ZnO/rGO composite. TEM images of (c) rGO, and (d) ZnO rods associated to rGO. (e) HR-TEM image of the ZnO/rGO composite and (f) the corresponding C-mapping.

der diffraction (XRD) diagrams of all samples were measured using Panalytical X'Pert Pro MPD diffractometer using Cu Kα radiation. The X-ray powder diffraction data were collected from an X'Pert MPD diffractometer (Panalytical AXS) with a goniometer radius 240 mm, fixed divergence slit module (1/2° divergence slit, 0.04 rd Sollers slits) and an X'Celerator as a detector. The powder samples were placed on a silicon zero-background sample holder and the XRD patterns were recorded at room temperature using Cu Kα radiation (λ = 0.15418 nm). The textural properties of the materials were investigated with a Micromeritics 3Flex Surface Characterization Analyzer instrument using liquid nitrogen (−196 °C). Prior to the analyzes, the samples were out-gassed overnight under primary vacuum at 40 °C on the ports of the Micromeritics VacPrep 061 degasser followed by 4 h out-gassing under high vacuum on the analyze ports. The resulting isotherms were analyzed using the BET (Brunauer-Emmett-Teller) method while the micropore volume (V_{micro}) was determined using the Horvath–Kawazoe (HK) equation. All the optical measurements were performed at room temperature (20 ± 1 °C) under ambient conditions. Absorption spectra of liquid samples were recorded on a Thermo Scientific Evolution 220 UV–vis spectrophotometer. The diffuse reflectance absorption spectra (DRS) were recorded on a Shimadzu 2600 UV–vis spectrophotometer. $BaSO_4$ powder was used as a standard for baseline measurements and spectra were recorded in a range of 250–1400 nm. Raman spectra were recorded using a Xplora spectrometer from Horiba Scientific with 532 nm wavelength incident laser light.

3. Results and discussion

3.1. Synthesis and characterization of ZnO/rGO composites

Fig. 1 describes the process for the preparation of ZnO/rGO composites. Graphite was first oxidized into graphite oxide *via* a modified Hummers method [55], followed by an exfoliation to generate graphene oxide (GO). Next, GO was reduced into rGO under mild conditions using an aqueous solution of sodium ascorbate [56]. rGO was next added to a mixture of $Zn(OAc)_2$ and NaOH in ethanol and the solution was sonicated 10 min to produce a homogeneous dispersion. The mixture was then transferred in a Teflon-sealed autoclave and heated at 160 °C to associate the formed ZnO nanorods with rGO using the functional groups remaining on rGO. In preliminary experiments, we varied the amount of rGO associated to ZnO (10, 20 or 40 wt% relative to ZnO) and found that photocatalysts prepared with 20 or 40 wt% in rGO adsorb high amounts of the Orange II dye during the adsorption–desorption phase preceding photocatalysis experiments (up to *ca.* 30%). Moreover, these photocatalysts exhibit a modest activity (see Fig. S1 for a comparison between the photocatalysts prepared with 10 and 40 wt% rGO). It is likely that the black rGO sheets in the ZnO/rGO composite increase photoabsorption and scattering leading to a decrease of the photocatalytic activity. Thus, a rGO loading of 10 wt% relative to ZnO was used in this study.

SEM and TEM experiments were first conducted to investigate the surface morphology, the size and the structure of ZnO, rGO and ZnO/rGO samples. Fig. 2a and b shows SEM images of ZnO rods prepared in the absence of rGO and of the ZnO/rGO composite, respectively. As can be seen, ZnO rods were successfully associated to rGO during the solvothermal synthesis. The surface of rGO sheets seems to be covered by densely packed ZnO rods which were not removed by centrifugation and washing of the composite, thus indicating a strong association between these two materials. No obvious differences in size could be observed between ZnO rods prepared in the absence or in the presence of rGO. Important informations of the ZnO/rGO composite were provided by TEM and HR-TEM analyzes. rGO exhibits a typical wrinkled texture and most of the sheets are curled and entangled together (Fig. 2c). The ZnO rods associated to rGO have an average length of *ca.* 180 nm and a diameter of *ca.* 16 nm (Fig. 2d). The associated EDS analysis proves that Zn, O and C are present in the composite (Fig. S2). The Zn/C molar ratio was found to be 4.51%. The HR-TEM image of the composite (Fig. 2e) and the corresponding C-mapping (Fig. 2f) conducted with Energy Filtered-TEM (EF-TEM) show the presence of a carbon layer with an average thickness of *ca.* 2 nm uniformly covering the ZnO rods and resulting in a sort of core/shell system.

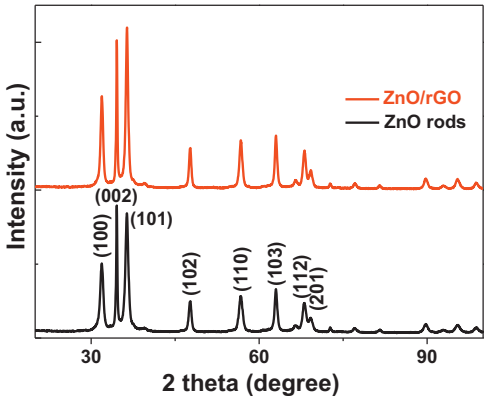

Fig. 3. XRD patterns of ZnO nanorods and of the ZnO/rGO composite.

The powder XRD patterns of ZnO nanotubes and of the ZnO/rGO composite are shown in Fig. 3. rGO typically exhibits two broad and weak diffraction peaks at 26° and 44.5° corresponding to the (0 0 2) and (1 0 0) planes, respectively [57]. These peaks were not detected in the ZnO/rGO composite, which might be due to the low content of rGO in the composite (4.51% based on EDS analysis) and/or to the low diffraction intensity of rGO compared to ZnO. The diffraction peaks at 2θ of 31.9°, 34.3°, 36.2°, 47.6°, 56.6°, 62.8°, 67.8° and 69.2° were respectively assigned to the (1 0 0), (0 0 2), (1 0 1), (1 0 2), (1 1 0), (1 0 3), (1 1 2) and (2 0 1) diffraction planes of hexagonal wurtzite structure ZnO (JCPDS No 36-1451). No diffraction peaks from other impurities were detected indicating that the ZnO/rGO composite was successfully prepared. It is also worth to mention that all diffraction peaks of ZnO in the ZnO/rGO composite did not shift to larger angles after their association with ZnO by heating at 160 °C for 24 h, thus indicating that a carbon-doping either on Zn or O sites is low under the synthetic conditions developed in this work [43,58,59].

The presence of rGO was first confirmed by Raman spectroscopy. The Raman-scattering spectra of GO, rGO, ZnO rods and of the ZnO/rGO composite recorded using a 532 nm laser light as an excitation source are shown in Fig. 4. The characteristic signals of D (vibration of defects states in graphene sheets) and G (bond stretching of sp^2 carbon atoms) bands of GO appear at 1335 and 1584 cm^{-1}, respectively, and the intensities ratio of these bands I_G/I_D is equal to 1.12. This ratio becomes close to 1 in rGO which indicates lower defects and disorders of the graphene structure and thus confirms the reduction of GO by ascorbic acid. For ZnO rods of wurtzite structure with $P6_3mc$ symmetry, the peaks at 325, 380 and 434 cm^{-1} can be assigned to *2E2* (*M*), *A1* (*TO*), and *E2* (*high*) vibration modes of ZnO, respectively [60]. All Raman signals relative to rGO and ZnO could clearly be observed in the ZnO/rGO composite. Finally, binding of rGO with ZnO rods resulted in a slight blue-shift of both the D and G bands (1346 and 1589 cm^{-1}, respectively) compared to rGO.

X-ray photoelectron spectra (XPS) of the ZnO/rGO composite was also recorded. From the full range spectrum of the composite (Fig. 5a), three dominate elements (Zn, O and C) can be

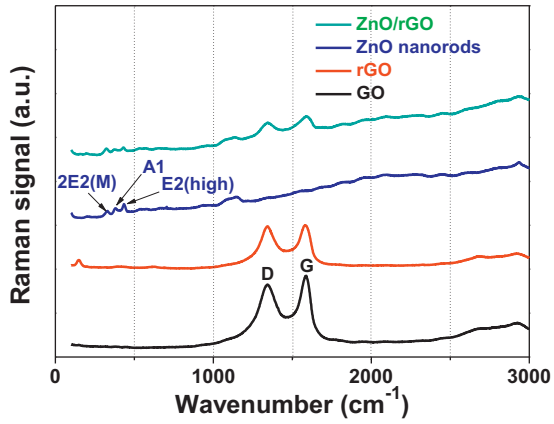

Fig. 4. Raman spectra of GO, rGO, ZnO rods and of the ZnO/rGO composite.

clearly observed, confirming the presence of ZnO and carbon in the sample. The C 1s XPS spectrum of the composite shows five main components corresponding to the various oxidation states of carbon in rGO: the C=C bonds non-linked to O (284.5 eV), the C—O bonds (epoxy and hydroxyl) (286.1 eV), the C=O at O—C—O bonds (287.5 eV), the carboxylate CO_2^- functions (288.6 eV) and finally at 290.1 eV, the π–π^* satellite peak of the aromatic conjugated domains modified with carboxylate, hydroxyl, and epoxide groups [61,62]. The latter signal confirms the existence of a partially modified π structure in the ZnO/rGO composite. Note that the intensities of peaks corresponding to C=O and CO_2^- functions are weak and that C—O bonds dominated. These results indicate that the mild chemical reduction of GO with sodium ascorbate is efficient for partially removing ketones and carboxylate functions but that epoxides and alcools remain unaffected by the reducing agent. The presence of O—C—O bonds in the ZnO/rGO composite indicates that the doping of ZnO rods originates from the substitution of Zn^{2+} atoms, which is in good accordance with XRD results and recent reports [43,59,63]. Only one peak located at 1022.1 eV is detected in the Zn 2p region and corresponds to Zn $2p_{3/2}$. The negative shift in the binding energy of Zn $2p_{3/2}$ in the ZnO/rGO compared to pure ZnO (1021.6 V) further confirms the association of ZnO with rGO. From the deconvolution of the O 1s region, two peaks were detected at 530.9 eV (Zn—O bonds) and 532.6 eV (C—O, C=O, and C—O—Zn bonds).

Along with the migration of electrons and holes induced by light, the optical absorption of the material is one of the key factors controlling photocatalytic reactions. Fig. 6 displays the UV–vis absorption spectra of ZnO rods, rGO and of the ZnO/rGO composite. For ZnO rods, a strong absorption located at *ca.* 360 nm originating from the intrinsic band-edge absorption of ZnO particles can be observed. This peak is slightly shifted in the ZnO/rGO composite due

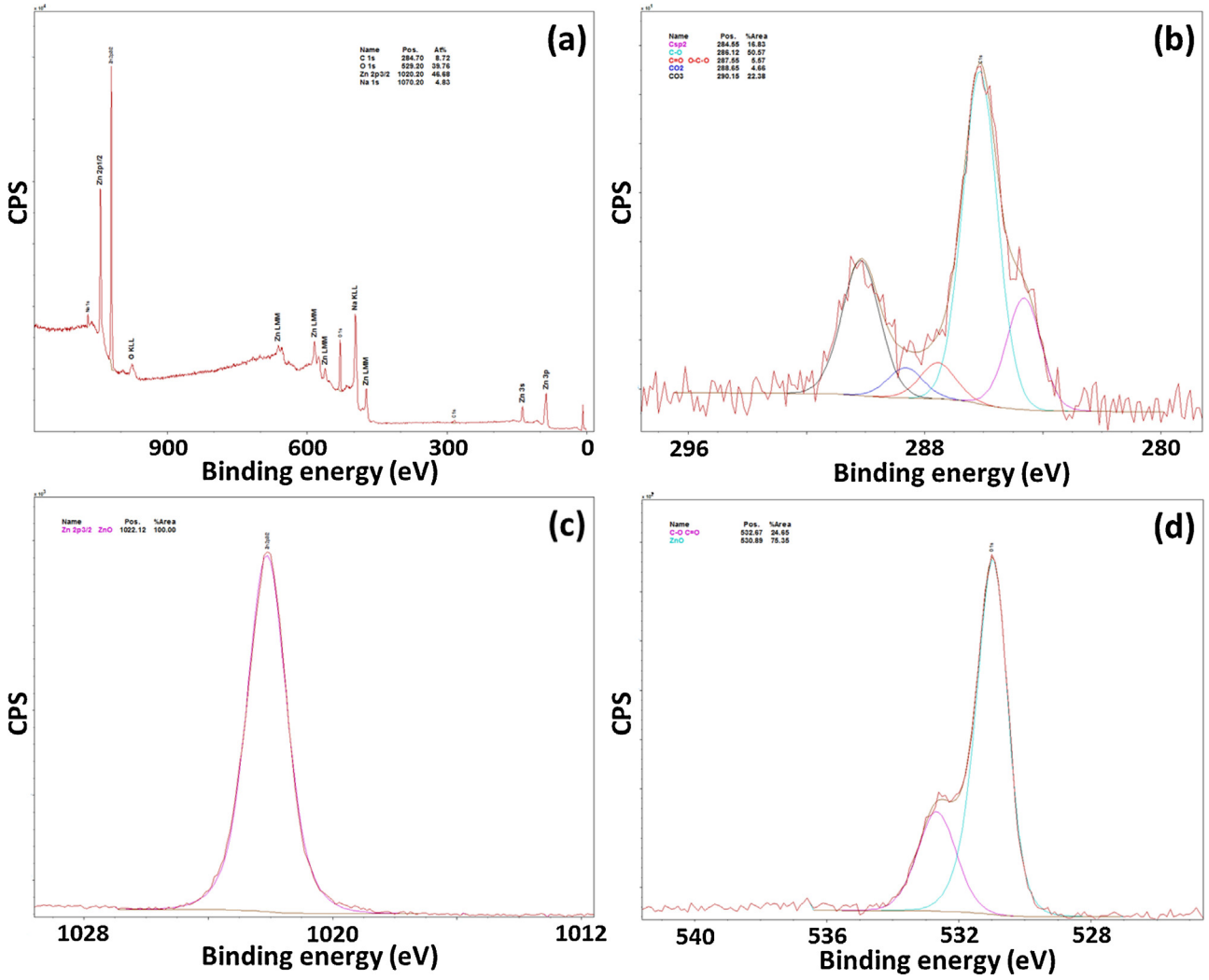

Fig. 5. XPS spectra of the ZnO/rGO composite. (a) overview, (b), (c) and (d) are the high-resolution spectra of C 1s, Zn 2p, and O 1s, respectively.

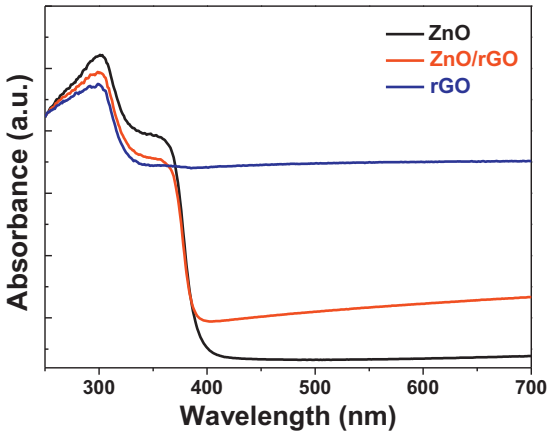

Fig. 6. UV–vis diffuse reflectance spectra of ZnO rods, rGO, and of the ZnO/rGO composite.

to a coupling effect originating from the interaction between ZnO rods and rGO [64,65]. The absorption peak located at 264 nm is generally associated to the excitation of the π-plasmon of the graphitic structure, and can be observed in rGO and in the ZnO/rGO composite [35]. By comparing the absorptions of ZnO and ZnO/rGO, it can be seen that absorption at wavelengths longer than 400 nm was much stronger in the ZnO/rGO composite due to the presence of rGO. This increase of absorption in the visible range is in accordance with the color change of the sample from white to grey and should have implications in the photocatalytic capability of the composite, especially under solar light irradiation. The decrease of reflectance and transmittance from 380 to 1400 nm for the ZnO/rGO composite may originate from the interface scattering caused by the porous structure of both ZnO rods and rGO and results in the increase of the optical path length. This scattering, also called light-trapping effect [66,67], can produce a longer path light inside the porous ZnO/rGO photocatalyst and thus increase its light absorption. This could also improve the photocatalytic efficiency of the ZnO/rGO composite (Fig. S3a–b). The diffuse reflectance spectra were used to estimate the bandgaps of ZnO and ZnO/rGO materials using the Kubelka-Munk function $K/S = F_{KM}(R) = (1-R)^2/2R$ [68]. The materials Eg were estimated from the plot $(F_{KM}(R)\cdot h\nu)^2$ versus hν using the Tauc relation. Because ZnO rods and rGO in the ZnO/rGO composite are different two phases, the bandgap energy of ZnO is not changed and was found to 3.3 eV for both materials (Fig. S3c–d) [39,69].

The BET surface areas of pure ZnO rods, rGO, and of the ZnO/rGO composite were investigated using nitrogen adsorption–desorption experiments (Fig. 7). The N_2 adsorption–desorption isotherms are of type III for ZnO and ZnO/rGO, and of type II for rGO, according to the Brunauer–Dening–Dening–Teller (BDDT) classification [70], indicating the presence of macropores. For rGO, the isotherms exhibit H4 hysteresis loops stopping at $P/P_0 = 0.42$, indicating the presence of micropores associated with sheet-like particles, giving rise to slit-like pores [71]. The desorption branch does not reach the adsorption branch, indicating a kinetic problem due to the presence of micropores, and attesting the presence of a microporosity. ZnO and ZnO/rGO materials exhibit high adsorption at relative pressures P/P_0 close to 1.0, suggesting the formation of large mesopores and macropores. This was further confirmed by the pore-size distribution of the samples which varied from 2 to 100 nm. The measured surface area of rGO is modest $75.77 \pm 0.35\ m^2/g$ (the theoretical specific surface area of rGO is $2600\ m^2/g$ [72]) likely due to the large amount of polar groups (hydroxyl, carbonyl,...) remaining on rGO after the

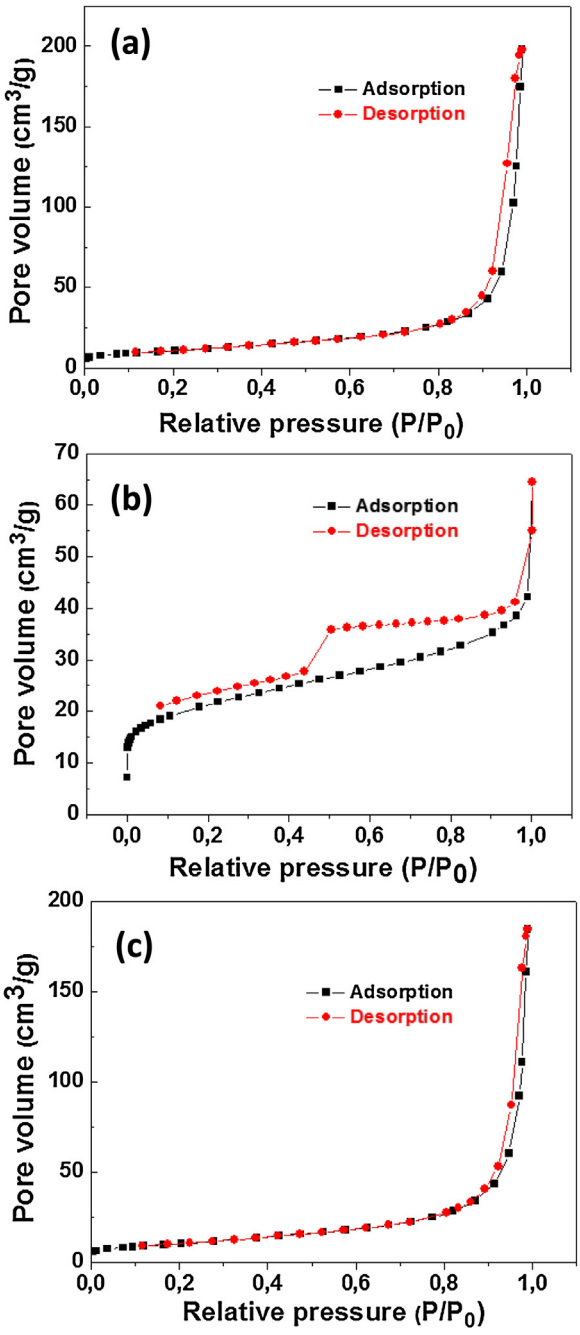

Fig. 7. Nitrogen adsorption–desorption isotherms of (a) ZnO rods, (b) rGO and (c) the ZnO/rGO composite.

mild reduction with ascorbic acid which caused tight hydrogen binding and strong sheet associations. The ZnO/rGO composite exhibits a similar surface area than ZnO rods (37.97 ± 0.24 and $36.93 \pm 0.27\ m^2/g$ for ZnO and ZnO/rGO, respectively) probably due to the low amount of rGO in the composite. However, the large specific surface of ZnO/rGO composite associated to its ability to transport charge carriers should be beneficial for enhancing the photocatalytic performances.

3.2. Photocatalytic experiments

The photocatalytic degradation of Orange II under simulated solar light was conducted to evaluate the performances on the ZnO/rGO composite. Prior to photocatalytic experiments, the dye

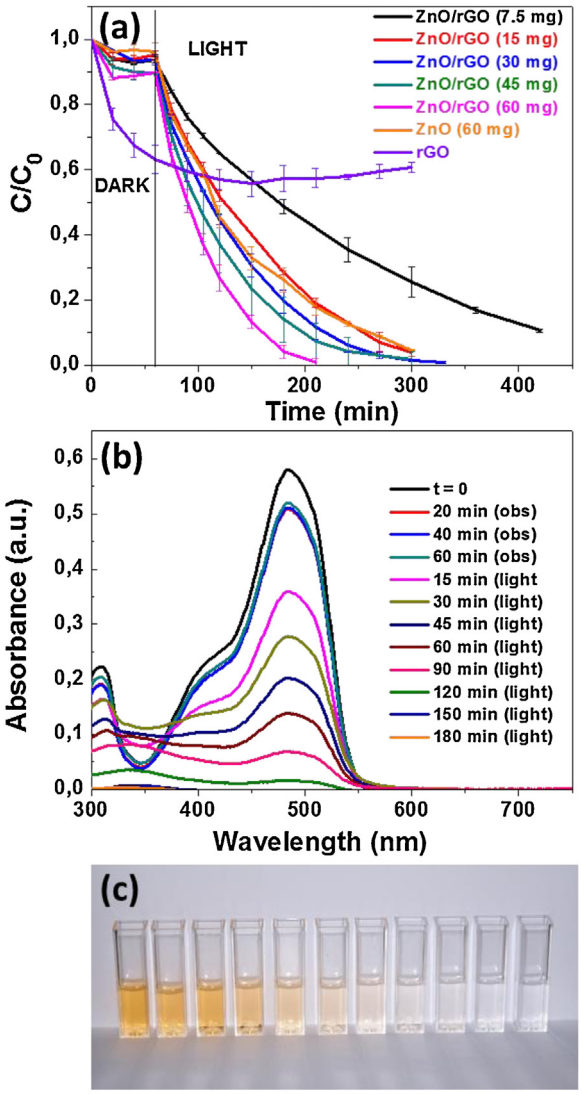

Fig. 8. (a) Influence of the ZnO/rGO photocatalyst mass for the degradation of Orange II in aqueous solution (C is the Orange II concentration at time t, and C_0 is the concentration of the dye at $t = 0$; volume of solution, 50 mL; Orange II concentration, 10 mg/L). (b) Variation of Orange II concentration as a function of irradiation time using 60 mg of photocatalyst. (c) Photographs of the Orange II solution during photocatalysis.

solution with the catalyst was kept in the dark for 60 min to attain the adsorption–desorption equilibrium of Orange II with the catalyst. In preliminary experiments, we determined that less of 1% of Orange II was decomposed *via* photolysis in the absence of catalyst after 2 h solar irradiation with a fluence of 5 mW/cm^2. A control experiment with rGO showed also that a strong adsorption (*ca.* 40% of the dye) occurred during the 60 min in the dark and that the concentration of Orange II remained quite unchanged under solar light irradiation (Fig. 8a).

3.2.1. *Influence of photocatalyst loading*

Because the photodegradation takes place on the surface of the catalyst, the degradation rate is expected to increase due to the increase of active sites. As can be seen from Fig. 8, with an increase of the ZnO/rGO composite loading from 7.5 to 60 mg in 50 mL of a 10 mg/L Orange II solution, the degradation kinetics gradually increased (*vide infra*) but the increase in catalyst loading did not significantly affect the percentage of Orange II degraded. Using 60 mg of the ZnO/rGO catalyst, the Orange II dye was nearly completely bleached after 150 min of solar light irradiation (Fig. 8b and c). In further experiments, 60 mg of the ZnO/rGO photocatalyst will be used. It is also worth to mention that the photocatalytic activity of the ZnO/rGO composite is markedly enhanced compared to ZnO rods (in both cases, 60 mg of catalyst in 50 mL of the Orange II solution). We also compared the photocatalytic efficiency of our ZnO/rGO to other catalysts associating rGO and ZnO rods previously described in the literature (note that methylene blue (MB) was used as dye in all these studies) [48,50,51]. Only under strong solar light irradiation, the complete photodegradation of MB could be achieved in short reaction times. In other reports, the conversion of MB never exceeded 88% even after prolonged reaction under UV light irradiation (up to 260 min). We attribute the high photocatalytic efficiency of our ZnO/rGO photocatalyst under mild (5 mW/cm^2) solar light irradiation to the effective decrease of charge carrier recombinations in this composite (*vide infra*).

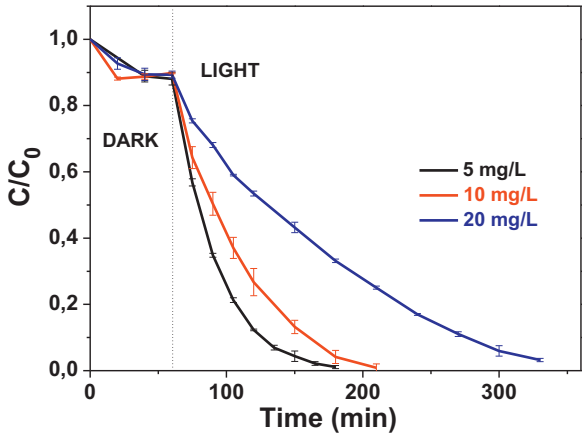

Fig. 9. Influence of the Orange II concentration of the catalytic activity of the ZnO/rGO photocatalyst (C is the Orange II concentration at time t, and C_0 is the concentration of the dye at $t = 0$; volume of solution, 50 mL; mass of ZnO/rGO catalyst, 60 mg).

The photocatalytic degradation of Orange II can be considered a pseudo-fist-order reaction. The efficiency of Orange II photodegradation by the ZnO/rGO composite was determined quantitatively using the pseudo-first-order model $\ln(C/C_0) = -kt$, where k is the apparent rate constant (min^{-1}) and C_0 and C are the concentrations of Orange II at time 0 and t, respectively. The rate constants k determined for the degradation of 50 mL of a 10 mg/L Orange II solution were found to be 0.0660, 0.0132, 0.0182, 0.0163, and 0.0292 min^{-1} when 7.5, 15, 30, 45, and 60 mg of the ZnO/rGO photocatalyst were used, respectively (See Fig. S4 for the plots of $\ln(C_0/C)$ *vs* reaction time).

Finally, we also evaluated the photodegradation of Orange II under visible light irradiation using a light intensity of 2 mW/cm^2 (Fig. S5). Data obtained showed that visible light can be used to bleach the dye but that the reaction requires a longer time compared to solar irradiation (*ca.* 40% of photodegradation after 4 h of visible irradiation) (Fig. S5).

3.2.2. *Effect of dye concentration*

The effect of the initial concentration of Orange II (5, 10 or 20 mg/L) on its degradation under solar light was also investigated (Fig. 9). Results obtained show that the decomposition rate of the dye depends on its initial concentration and that the efficiency of photodegradation decreases with the increase of the dye concentration ($k = 0.0334$, 0.0237 and 0.0104 min^{-1} for Orange II concentrations of 5, 10, and 20 mg/L, respectively) (See Fig. S6 for the plots of $\ln(C_0/C)$ *vs* reaction time). An increase of the initial Orange II concentration results in an increase of the amount of dye adsorbed on the catalyst surface, and thus to a decrease of the catalyst activity. The increase of the dye concentration can also generate

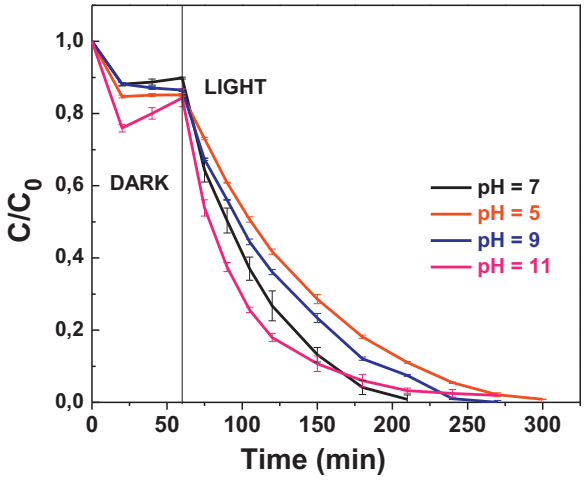

Fig. 10. Influence of pH on the photodegradation of Orange II by the ZnO/rGO composite under solar light irradiation (volume of solution, 50 mL; Orange II concentration, 10 mg/L; mass of catalyst, 60 mg).

a filter effect which decreases the amount of incident light wasted for the dye excitation rather than reactive oxygen species (ROS) production.

3.2.3. Influence of the pH

The pH of the dye solution is an important factor in the reaction taking place on photocatalysts surfaces since it is related to the surface charge properties. The ZnO/rGO composite exhibits an excellent photocatalytic activity toward the bleaching of Orange II at a wide pH range varying from 5 to 11 (Fig. 10). After 150 min of irradiation, the percentages of degradation were 99, 97, 93 and 89% when the ZnO/rGO catalyst was used at pH = 7, 11, 9, and 5, respectively. The kinetic of the degradation during the first 115 min of irradiation is increased at pH = 11. The enhancing effect of increasing pH probably originates from a more efficient formation of hydroxyl radical •OH from HO^- than from H_2O.

3.2.4. Influence of ions and molecules on the photocatalytic efficiency

Salts commonly present in wastewater may also strongly affect photocatalytic efficiency due to their competitive adsorption on the catalyst and due to their ability to trap ROS [73]. In a first set of experiments, NaCl, $CaCl_2$, $MgCl_2$, Na_2SO_4 or $NaNO_3$ were added to the Orange II solution at a 10 mM concentration and at neutral pH before conducting photocatalytic experiments (Fig. 11a). As can be seen, the presence of Na_2SO_4 had no influence on the ZnO/rGO catalyst activity, while NaCl, $CaCl_2$, $MgCl_2$ and $NaNO_3$ increased the rate of the Orange II degradation. The amount of dye adsorbed by the photocatalyst is also slightly increased in the presence of $CaCl_2$ probably due to electrostatic interactions between the negatively charged ZnO, Ca^{2+}, and the anionic Orange II dye.

This phenomenon is enhanced in the presence of Fe^{3+} and especially Fe^{2+} both used at a 100 μM concentration (Fig. 11b). Moreover, the kinetic of degradation increases markedly in the presence of Fe^{2+}. This may originate from the ability of Fe^{2+} to generate •OH radicals from H_2O_2 *via* a Fenton reaction [74]. Finally, Zn^{2+} ions (100 μM) and the reducing sugar glucose (50 mg/L) only slightly reduced the degradation rate.

3.2.5. Recycling of the catalyst

In addition to photocatalytic activity, the stability of the photocatalyst is another important issue for its practical application. The catalytic test using the ZnO/rGO composite to investigate the recyclability and stability in repeated Orange II degradation

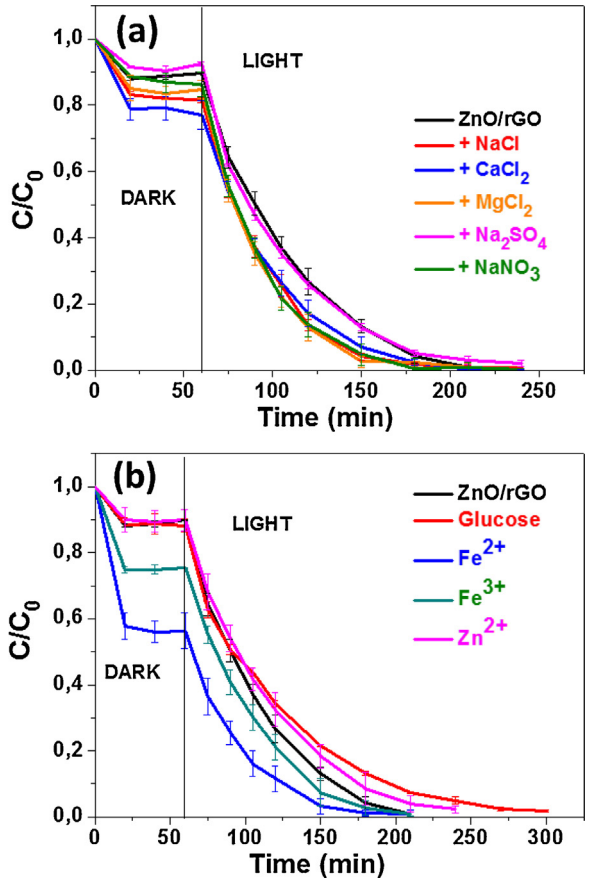

Fig. 11. Effects of salts and of glucose on the photocatalytic efficiency of the ZnO/rGO composite used under solar light irradiation (volume of solution, 50 mL; Orange II concentration, 10 mg/L; mass of catalyst, 60 mg).

experiments. After each reaction, the catalyst was collected by centrifugation, washed with water and subsequently dried at 60 °C for 12 h before its reuse. As shown in Fig. 12a, 95% of Orange II was photo-degraded in 2 h after the first cycle. After 15 reuses, the photocatalytic activity only slightly decreased and *ca.* 89% of the dye were bleached after the same reaction time. The slight decrease of activity demonstrates that the photocatalyst has a high repeatability. A SEM image of the recycled catalyst is shown in Fig. 12b and obviously indicates that no aggregation of ZnO rods occurred during photocatalysis.

3.2.6. Photocatalytic mechanism

The formation of ROS such as hydroxyl radicals (•OH) and superoxide ($O_2^{-\bullet}$) radicals under photocatalytic conditions and their role in the Orange II dye degradation process has been investigated indirectly with the use of appropriate quenchers of these species. In these experiments, a comparison is made between the degradation curve determined with the ZnO/rGO composite with those obtained after addition of quenchers in the initial solution under otherwise identical conditions. Compounds used for this purpose were *t*-BuOH, a •OH radical scavenger, and benzoquinone, which is a $O_2^{\bullet-}$ quencher [75]. In the presence of benzoquinone (5 mg in 50 mL of the Orange II solution), the transformation of Orange II is completely suppressed indicating that $O_2^{\bullet-}$ radicals anions play a key role in the photocatalytic degradation. Note that the absorption at 485 nm slightly increases during this experiment due to the polymerization of benzoquinone into oligohydroquinones which strongly absorb at this wavelength. When the photocatalysis was conducted in the presence of *t*-BuOH (300 μL in 50 mL of the Orange II solution), the degradation rate obviously decreased

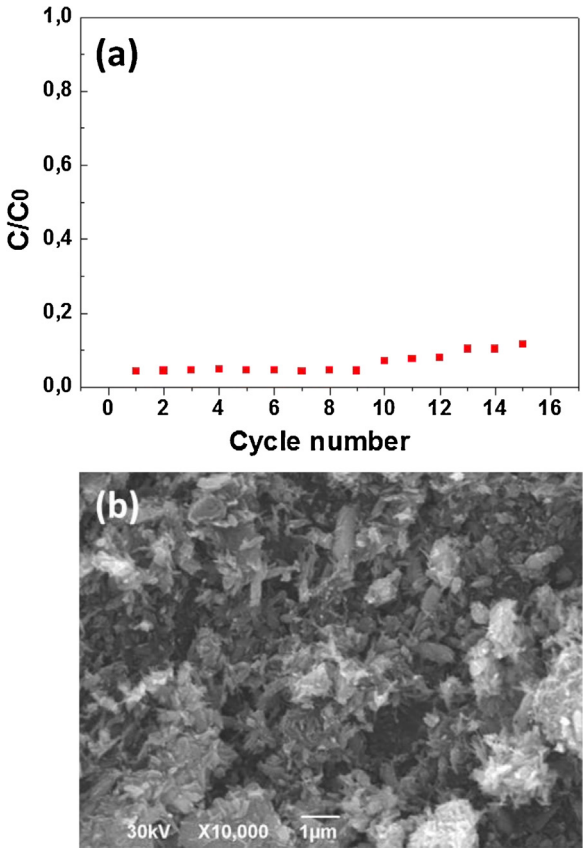

Fig. 12. (a) Values of C/C_0 during the recycling of the ZnO/rGO photocatalyst. (b) SEM image of the photocatalyst after 15 reuses.

but the photocatalytic activity was not suppressed (Fig. 13). These results demonstrate that •OH and $O_2^{\bullet -}$ are major species in the Orange II degradation reactions.

The proposed reaction mechanism for the ZnO/rGO photocatalyst is schematically illustrated in Fig. 14. Upon simulated solar light irradiation, electrons (e^-) are photo-generated from the valence band to the conduction band of ZnO rods. These e^- are next transferred to rGO which efficiently separates them and minimizes the charge recombination processes, thus enhancing the photocatalytic performances. The e^- captured by rGO reacted with O_2 to form $O_2^{\bullet -}$ while the holes in ZnO generate •OH radicals. As highly reactive species, •OH and $O_2^{\bullet -}$ radicals oxidize the Orange II dye into water, carbon dioxide and inorganic salts.

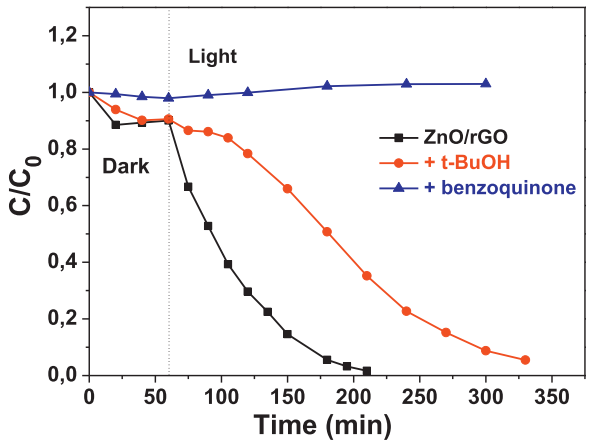

Fig. 13. Influence of *t*-BuOH and benzoquinone used as OH and $O_2^{\bullet -}$ scavengers, respectively, on the photocatalytic activity of the ZnO/rGO composite.

4. Conclusions

ZnO nanorods with an average length of *ca.* 180 nm and a diameter of *ca.* 16 nm and associated to rGO were synthesized using a solvothermal method. The photocatalytic performances were found to depend on the amount of rGO associated to ZnO. The ZnO/rGO composite with 10 wt% rGO was found to achieve the highest removal of Orange II (99% of degradation under solar light irradiation after 150 min). Moreover, the ZnO/rGO photocatalyst was found to be weakly sensitive to salts commonly present in wastewater and to pH changes and could be reused up to 15 times without significant loss of catalytic activity. The increased light absorption intensity and range and the reduced charge recombination generated by the association of ZnO rods with rGO are responsible for the highest catalytic activity of the ZnO/rGO composite compared to ZnO rods. We hope that the solvothermal synthetic method developed in this work for the production of high quality ZnO rods associated to rGO is a promising technique for the preparation of efficient photocatalysts for the removal of pollutants.

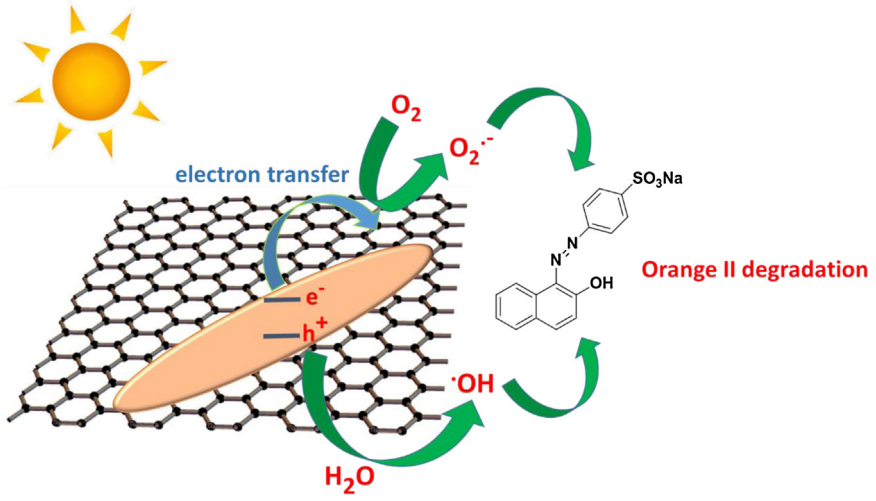

Fig. 14. Possible mechanism for the degradation of Orange II with the ZnO/rGO composite under solar light irradiation.

Acknowledgements

This work is supported by the Agence Nationale pour la Recherche (ANR CESA 2011, project NanoZnOTox). We also acknowledge the competitive cluster Hydreos for its support. We thank Jaafar Ghanbaja (IJL, UMR CNRS 7198, Université de Lorraine) for HR-TEM experiments.

Appendix A. Supplementary data

Supplementary data associated with this article can be found, in the online version, at http://dx.doi.org/10.1016/j.apcatb.2015.12.007.

References

[1] E.S. Jang, J.H. Won, S.J. Hwang, J.H. Choy, Fine tuning of the face orientation of ZnO crystals to optimize their photocatalytic activity, Adv. Mater. 18 (18) (2006) 3309–3312.
[2] S. Chakrabarti, B.K. Dutta, Photocatalytic degradation of model textile dyes in wastewater using ZnO as semiconductor catalyst, J. Hazard. Mater. 112 (2004) 269–278.
[3] N. Kislov, J. Lahiri, H. Varma, D.Y. Goswami, E. Stefanakos, M. Batzill, Photocatalytic degradation of methyl orange over single crystalline ZnO: orientation dependence of photoactivity and photostability of ZnO, Langmuir 25 (2009) 3310–3315.
[4] H. Labiadh, T. Ben Chaabane, L. Balan, N. Becheick, S. Corbel, G. Medjahdi, R. Schneider, Preparation of Cu-doped ZnS QDs/TiO_2 nanocomposites with high photocatalytic activity, Appl. Catal. B: Environ. 144 (2014) 29–35.
[5] L. Li, X. Liu, Y. Zhang, N.T. Nuhfer, K. Barmak, P.A. Salvador, G.S. Kohrer, Visible-light photochemical activity of heterostructured core–shell materials composed of selected ternary titanates and ferrites coated by TiO_2, ACS Appl. Mater. Interfaces 5 (2013) 5064–5071.
[6] K. Navaveni, G. Silvalingam, M.S. Hedge, G. Madros, Photocatalytic degradation of organic compounds over combustion-synthesized nano-TiO_2, Environ. Sci. Technol. 38 (2004) 1600–1604.
[7] A.L. Linsebrigler, G. Lu, J.T. Yates, Photocatalysis on TiO_2 surfaces: principles, mechanisms, and selected results, Chem. Rev. 95 (1995) 735–758.
[8] F. Achouri, S. Corbel, A. Aboulaich, L. Balan, A. Ghrabi, M. Ben Said, R. Schneider, Aqueous synthesis and enhanced photocatalytic activity of ZnO/Fe_2O_3 heterostructures, J. Phys. Chem. Solids 75 (2014) 1081–1087.
[9] S. Dong, J. Feng, M. Fan, Y. PI, L. Hu, X. Han, M. Liu, J. Sun, Recent developments in heterogeneous photocatalytic water treatment using visible light-responsive photocatalysts: a review, RSC Adv. 5 (2015) 14610–14630.
[10] F. Li, Y. Ding, P.X. Gao, X.Q. Xin, Z.L. Wang, Single-crystal hexagonal disks and rings of ZnO: low-temperature, large-scale synthesisand growth mechanism, Angew. Chem. Int. Ed. 43 (2004) 5238–5242.
[11] N. Sinha, G. Ray, S. Bhandari, S. Godara, B. Kumar, Synthesis and enhanced properties of cerium doped ZnO nanorods, Ceram. Int. 40 (2014) 12337–12342.
[12] H. Yin, K. Yu, J. Hu, C. Song, B. Guo, Z. Wang, Z. Zhu, Novel photoluminescence properties and enhanced photocatalytic activities for V_2O_5-loaded ZnO nanorods, Dalton Trans. 44 (2015) 4671–4678.
[13] Q. Jiang, Y. Liu, H. Kan, B. Yuan, H. Zhao, Microwave-assisted synthesis of hexagonal structure ZnO micro-tubes, Mater. Lett. 81 (2012) 198–201.
[14] H. Zhang, D. Yang, Y. Ji, X. Ma, J. Xu, D. Que, Low temperature synthesis of flowerlike ZnO nanostructures by cetyltrimethylammonium bromide-assisted hydrothermal process, J. Phys. Chem. B 108 (2004) 3955–3958.
[15] S.-M. Lam, J.C. Sin, I. Satoshi, A.Z. Abdullah, A.R. Mohamed, Enhanced sunlight photocatalytic performance over Nb_2O_5/ZnO nanorod composites and the mechanism study, Appl. Catal. A: Gen. 471 (2014) 126–135.
[16] M.-H. Hsu, C.-J. Chang, Ag-doped ZnO nanorods coated metal wire meshes as hierarchical photocatalysts with high visible-light driven photoactivity and photostability, J. Hazard. Mater. 278 (2014) 444–453.
[17] J. Fang, H. Fan, G. Dong, A facile way to synthesize cost-effective ZnO nanorods with enhanced photocatalytic activity, Mater. Lett. 120 (2014) 147–150.
[18] B.M. Rajbongshi, S.K. Samdarshi, ZnO and Co-ZnO nanorods-Complementary role of oxygen vacancy in photocatalytic activity of under UV and visible radiation flux, Mater. Sci. Eng. B 182 (2014) 21–28.
[19] S. Khanchandani, P.K. Srivestava, S. Kumar, S. Ghosh, A.K. Ganguli, Band gap engineering of ZnO using core/shell morphology with environmentally benign Ag_2S sensitizer for efficient light harvesting and enhanced visible-light photocatalysis, Inorg. Chem. 53 (2014) 8902–8912.
[20] A. McLaren, T. Valdes-Solis, G. Li, S.C. Tsang, Shape and size effects of ZnO nanocrystals on photocatalytic activity, J. Am. Chem. Soc. 131 (2009) 12540–12541.
[21] Y. Zheng, C. Chen, Y. Zhan, X. Lin, Q. Zheng, K. Wei, J. Zhu, Y. Zhu, Y. Zheng, Luminescence and photocatalytic activity of ZnO nanocrystals: correlation between structure and property, Inorg. Chem. 46 (2007) 6675–6682.
[22] D. Wu, W. Wang, F. Tan, F. Sun, H. Lu, X. Qiao, Fabrication of pit-structured ZnO nanorods and their enhanced photocatalytic performance, RSC Adv. 3 (2013) 20054–20059.
[23] Y. Peng, S. Qin, W.-S. Wang, A.-W. Xu, Fabrication of porous Cd-doped ZnO nanorods with enhanced photocatalytic activity and stability, CrystEngComm 15 (2013) 6518–6525.
[24] O. Akhavan, M. Mehrabian, K. Mirabbaszadeh, R. Azimirad, Hydrothermal synthesis of ZnO nanorod arrays for photocatalytic inactivation of bacteria, J. Phys. D: Appl. Phys. 42 (2009) 225305.
[25] S. Baruah, M. Abbas Mahmood, M.T. Zar Myint, T. Bora, J. Dutta, Enhanced visible light photocatalysis through fast crystallization of zinc oxide nanorods, Beilstein J. Nanotechnol. 1 (2010) 14–20.
[26] X. Qiu, G. Li, X. Sun, L. Li, X. Fu, Doping effects of Co^{2+} ions on ZnO nanorods and their photocatalytic properties, Nanotechnology 19 (2008) 215703.
[27] L. Jiang, L. Gao, Fabrication and characterization of ZnO-coated multi-walled carbonnanotubes with enhanced photocatalytic activity, Mater. Chem. Phys. 91 (2005) 313–316.
[28] X.J. Wang, S.W. Yao, X.B. Li, Sol–gel preparation of CNT/ZnO nanocomposite and its photocatalytic property, Chin. J. Chem. 27 (2009) 1317–1320.
[29] L.P. Zhu, G.H. Liao, W.Y. Huang, L.L. Ma, Y. Yang, Y. Yu, S.Y. Fu, Preparation, characterization and photocatalytic properties of ZnO-coatedmulti-walled carbon nanotubes, Mater. Sci. Eng. B 163 (2009) 194–198.
[30] J. Mu, C. Shao, Z. Guo, Z. Zhang, M. Zhang, P. Zhang, B. Chen, Y. Liu, High photocatalytic activity of ZnO-carbon nano fiber hetero architectures, ACS Appl. Mater. Interfaces 3 (2011) 590–596.
[31] Y. Yan, T. Chang, P.C. Wei, S.Z. Kang, J. Mu, Photocatalytic activity of nanocomposites of ZnO and multi-walled carbon nanotubes for dye degradation, J. Dispersion Sci. Technol. 30 (2009) 198–203.
[32] P. Wang, Y. Zhai, D. Wang, S. Dong, Synthesis of reduced graphene oxide-anatase TiO_2 nanocomposite and its improved photo-induced charge transfer properties, Nanoscale 3 (2011) 1640–1645.
[33] C.-J. Chang, K.-W. Chu, M.-H. Hsu, C.-Y. Chen, Ni-doped ZnS decorated graphene composites withenhanced photocatalytic hydrogen-production performance, Int. J. Hydrogen Energy 40 (2015) 14498–14506.
[34] I.V. Lightcap, T.H. Kosel, P.V. Kamat, Anchoring semiconductor and metalnanoparticles on a two-dimensional catalystmat. storing and shuttling electrons with reduced graphene oxide, Nano Lett. 10 (2010) 577–583.
[35] J. Wu, X. Shen, L. Jiang, K. Wang, K. Chen, Solvothermal synthesis and characterization of sandwich-like graphene/ZnO nanocomposites, Appl. Surf. Sci. 256 (2010) 2826–2830.
[36] O. Akhavan, Photocatalytic reduction of graphene oxides hybridized by ZnO nanoparticles in ethanol, Carbon 49 (2011) 11–18.
[37] X. Liu, L. Pan, T. Lv, T. Lu, G. Zhu, Z. Sun, C. Sun, Microwave-assisted synthesis of ZnO–graphene composite forphotocatalytic reduction of Cr(VI), Catal. Sci. Technol. 1 (2011) 1189–1193.
[38] H. Hayashi, I.V. Lightcap, M. Tsujimoto, M. Takano, T. Umeyama, P.V. Kamat, H. Imahori, Electron transfer cascade by organic/inorganic ternary composites of porphyrin, zinc oxide nanoparticles, and reduced grapheneoxide on a tin oxide electrode that exhibits efficient photo current generation, J. Am. Chem. Soc. 133 (2011) 7684–7687.
[39] T. Xu, L. Zhang, H. Cheng, Y. Zhu, Significantly enhanced photocatalytic performance of ZnO via graphene hybridization and the mechanism study, Appl. Catal. B: Environ. 101 (2011) 382–387.
[40] B. Li, T. Liu, Y. Wang, Z. Wang, ZnO/graphene-oxide nanocomposite with remarkably enhanced visible-light-driven photocatalytic performance, J. Colloid Interface Sci. 377 (2012) 114–121.
[41] X. Liu, L. Pan, Q. Zhao, T. Lv, G. Zhu, T. Chen, T. Lu, Z. Sun, C. Sun, UV-assisted photocatalytic synthesis of ZnO–reduced graphene oxide compositeswith enhanced photocatalytic activity in reduction of Cr(VI), Chem. Eng. J. 183 (2012) 238–243.
[42] J. Wang, T. Tsuzuki, B. Tang, X. Hou, L. Sun, X. Wang, Reduced graphene oxide/ZnO composite: reusable adsorbent for pollutant management, ACS Appl. Mater. Interfaces 4 (2012) 3084–3090.
[43] Z. Zhan, L. Zheng, Y. Pan, G. Sun, L. Li, Self-powered, visible-light photodetector based on thermally reduced grapheneoxide–ZnO (rGO–ZnO) hybrid nanostructure, J. Mater. Chem. 22 (2012) 2589–2595.
[44] S. Liu, H. Sun, A. Suvorova, S. Wang, One-pot hydrothermal synthesis of ZnO-reduced graphene oxidecomposites using Zn powders for enhanced photocatalysis, Chem. Eng. J. 229 (2013) 533–539.
[45] Y. Wang, F. Wang, J. He, Controlled fabrication and photocatalytic properties of a three-dimensional ZnO nanowire/reduced grapheneoxide/CdS heterostructure on carbon cloth, Nanoscale 5 (2013) 11291–11297.
[46] Y. Cheng, Y. Fan, Y. Pei, M. Qiao, Graphene-supported metal/metal oxide nanohybrids: synthesisand applications in heterogeneous catalysis, Catal. Sci. Technol. 5 (2015) 3903–3916.
[47] O. Akhavan, Graphene nanomesh by ZnO nanorod photocatalysts, ACS Nano 10 (2010) 4174–4180.
[48] T. Lv, L. Pan, X. Liu, T. Lu, G. Zhu, Z. Sun, Enhanced photocatalytic degradation of methylene blue by ZnO-reduced graphene oxide composite synthesized via microwave-assisted reaction, J. Alloys Compd. 509 (2011) 10086–10091.
[49] T. Lv, L. Pan, X. Liu, Z. Sun, Enhanced photocatalytic degradation of methylene blue by ZnO–reduced graphene oxide-carbon nanotube compositessynthesized via microwave-assisted reaction, Catal. Sci. Technol. 2 (2012) 2297–2301.

[50] X. Zhou, T. Shi, H. Zhou, Hydrothermal preparation of ZnO-reduced graphene oxide hybrid with high performance in photocatalytic degradation, Appl. Surf. Sci. 258 (2012) 6204–6211.
[51] H. Sun, S. Liu, S. Liu, S. Wang, A comparative study of reduced graphene oxide modified TiO_2, ZnO and Ta_2O_5 in visible light photocatalytic/photochemical oxidation of methylene blue, Appl. Catal. B: Environ. 146 (2014) 162–168.
[52] R.C. Pawar, C.S. Lu, Single-step sensitization of reduced graphene oxide sheets and CdS nanoparticles on ZnO nanorods as visible-light photocatalysts, Appl. Catal. B: Environ. 144 (2014) 57–65.
[53] Y. Zheng, C. Chen, Y. Zhan, X. Lin, Q. Zheng, K. Wei, J. Zhu, Y. Zhu, Luminescence and photocatalytic activity of ZnO nanocrystals:correlation between structure and property, Inorg. Chem. 46 (2007) 6675–6682.
[54] M.Y. Guo, A.M. Ching Ng, F. Liu, A.B. Djurisic, W.K. Chan, H. Su, K.S. Wong, Effect of native defects on photocatalytic properties of ZnO, J. Phys. Chem. C 115 (2011) 11095–11101.
[55] K. Wang, J. Ruan, H. Song, J. Zhang, Y. Wo, S. Guo, D. Cui, Biocompatibility of graphene oxide, Nanoscale Res. Lett. 6 (2011) 8.
[56] J. Zhang, H. Yang, G. Shen, P. Cheng, J. Zhang, S. Guo, Reduction of graphene oxide via L-ascorbic acid, Chem. Commun. 46 (2010) 1112–1114.
[57] L. Tang, Y. Wang, Y. Li, H. Feng, J. Lu, J. Li, Preparation, structure, and electrochemical properties of reduced graphene sheet films, Adv. Funct. Mater. 19 (2009) 2782–2789.
[58] S. Cho, J.W. Jang, J.S. Lee, K.H. Lee, Carbon-doped ZnO nanostructures synthesized using vitamin C for visible light photocatalysis, CrystEngComm 12 (2010) 3929–3935.
[59] S. Akbar, S.K. Hasanain, M. Abbas, S. Ozcan, B. Ali, S.I. Shah, Defect induced ferromagnetism in carbon-doped ZnO thin films, Solid State Commun. 151 (2011) 17–20.
[60] K.A. Alim, V.A. Fonoberov, M. Shamsa, A.A. Baladin, Micro-Raman investigation of optical phonons in ZnO nanocrystals, J. Appl. Phys. 97 (2005) 124313.
[61] E.C. Onyiriuka, AM 2001 lubricant film on canasite glass–ceramic magnetic memory disk, Chem. Mater. 5 (1993) 798–801.
[62] X.Z. Zhou, X. Huang, X.Y. Qi, S.X. Wu, C. Xue, F.Y.C. Boey, Q.Y. Yan, P. Chen, H. Zhang, In situ synthesis of metal nanoparticles on single-layer graphene oxide and reduced graphene oxide surfaces, J. Phys. Chem. C 113 (2009) 10842–10846.
[63] S.T. Tan, X.W. Sun, Z.G. Yu, P. Wu, G.Q. Lo, D.L. Kwong, *p*-type conduction in unintentional carbon-doped ZnO thin films, Appl. Phys. Lett. 91 (2007) 072101.
[64] R.C. Wang, Y.C. Chen, S.J. Chen, Y.M. Chang, Unusual functionalization of reduced graphene oxide for excellent chemical surface-enhanced Raman scattering by coupling with ZnO, Carbon 70 (2014) 215–233.
[65] Y. Li, Z. Zeng, J. Zhu, S. Chen, X. Yuan, S. Liu, Graphene nanosheets decorated with ZnO nanoparticles: facile synthesis and promising application for enhancing the mechanical and gas barrier properties of rubber nanocomposites, RSC Adv. 5 (2015) 57771–57780.
[66] C.-J. Chang, E.-H. Kuo, Light-trapping effects and dye adsorption of ZnO hemisphere-array surfacecontaining growth-hindered nanorods, Colloids Surf A: Physicochem. Eng. Aspects 363 (2010) 22–29.
[67] S.-T. Hung, C.-J. Chang, M.-H. Hsu, Improved photocatalytic performance of ZnO nanograss decorated pore-arrayfilms by surface texture modification and silver nanoparticle deposition, J. Hazard. Mater. 198 (2011) 307–316.
[68] Y.P. Zhang, C.X. Pan, TiO_2/graphene composite from thermal reaction of grapheneoxide and its photocatalytic activity in visible light, J. Mater. Sci. 46 (2011) 2622–2626.
[69] H. Zhang, X.J. Lv, Y.M. Li, Y. Wang, J.H. Li, P25-graphene composite as a high performance photocatalyst, ACS Nano 4 (2010) 380–386.
[70] K. Singh, D. Everett, R. Haul, L. Moscou, R. Pierotti, J. Rouquerol, T. Siemieniewska, Reporting physisorption data for gas/solid systems with special reference to the determination of surface area and porosity, Pure Appl. Chem. 57 (1985) 603–619.
[71] X.X. Yu, J.G. Yu, B. Cheng, M. Jaroniec, Synthesis of hierarchical flower-like AlOOH and TiO_2/AlOOH superstructures and their enhanced photocatalytic properties, J. Phys. Chem. C 113 (2009) 17527–17535.
[72] O. Akhavan, E. Ghaderi, Photocatalytic reduction of graphene oxide nanosheets on TiO_2 thin film for photoinactivation of bacteria in solar light irradiation, J. Phys. Chem. C 113 (2009) 20214–20220.
[73] A. Aguedach, S. Brosillon, J. Morvan, E.K. Lhadi, Influence of ionic strength in the adsorption and during photocatalysisof reactive black 5 azo dye on TiO_2 coated on nonwoven paper with SiO_2 as a binder, J. Hazard. Mater. 150 (2008) 250–256.
[74] B. Tryba, A.W. Morawski, M. Inagaki, M. Toyoda, The kinetics of phenol decomposition under UV irradiation with andwithout H_2O_2 on TiO_2, Fe–TiO_2 and Fe–C–TiO_2 photocatalysts, Appl. Catal. B: Environ. 63 (2006) 215–221.
[75] C. Hu, T. Peng, X. Hu, Y. Nie, X. Zhou, J. Qu, H. He, Plasmon-induced photodegradation of toxic pollutants with Ag-AgI/Al2O3 under visible-light irradiation, J. Am. Chem. Soc. 132 (2010) 857–862.